Lattice defects induce microtubule self-renewal

Laura Schaedel,[1] Sarah Triclin,[1] Denis Chrétien,[2] Ariane Abrieu,[3] Charlotte Aumeier,[1]
Jérémie Gaillard,[1] Laurent Blanchoin,[4,*] Manuel Théry,[4,†] and Karin John[5,‡]

[1]*Univ. Grenoble-Alpes, CEA, CNRS, INRA, Biosciences & Biotechnology Institute of Grenoble, Laboratoire de Physiologie Cellulaire & Végétale, CytoMorpho Lab, 38054 Grenoble, France.*
[2]*Univ. Rennes, CNRS, IGDR (Institute of Genetics and Development of Rennes) - UMR6290, F-35000 Rennes, France.*
[3]*CRBM, CNRS, University of Montpellier, Montpellier, France.*
[4]*Univ. Paris Diderot, INSERM, CEA, Hôpital Saint Louis, Institut Universitaire d'Hematologie, UMRS1160, CytoMorpho Lab, 75010 Paris, France.*
[5]*Univ. Grenoble-Alpes, CNRS, Laboratoire Interdisciplinaire de Physique, 38000 Grenoble, France.*

Supplementary Information

I. ESTIMATION OF THE TYPICAL TIME SCALE OF DIMER EXCHANGE AT THE PERFECT LATTICE

In a fully occupied lattice the binding energy ΔG_B of a dimer is about -45 to -65 k_BT, assuming an entropic loss ΔG_E of 10 to 20 k_BT upon transferring a dimer from the solution into the lattice [1, 2]. These estimates have been obtained by fitting the measured tip dynamics to a kinetic model. In contrast, calculations based on a Poisson-Boltzmann model on the atomic scale have estimated a binding energy of about -90 k_BT [3]. The typical time τ for the loss of a single dimer from the shaft of a 20 μm long 13 protofilament microtubule (containing N=13*125*20=32500 dimers) can be estimated from the principle of detailed balance [cf. Eq. (1) in Methods] as $1/\tau = k_{on} c_0 N e^{(\Delta G_B + \Delta G_E)/k_BT}$. Thereby k_{on}=5 x $10^6\,\mathrm{M}^{-1}\,\mathrm{s}^{-1}$ denotes the on-rate constant [4] with the standard concentration c_0=1 M. Using the lower estimates ΔG_B=-45 k_BT and ΔG_E=10 k_BT we find a typical time $\tau \approx 3$ hours. However, a small energy decrease of the binding energy of about 2.5 k_BT (This corresponds e.g. roughly to the difference in the lattice energy between a GDP and GTP-lattice [1]) reduces the typical time τ to 15 minutes, since the energy dependence of the rate constants is exponential. As an illustration, Supplementary Fig. S2a shows the dependence of τ on ΔG_B and ΔG_E.

II. SIMULATIONS AND EXPERIMENTS OF MICROTUBULE LATTICE DYNAMICS IN THE ABSENCE OF FREE TUBULIN

We have further tested the model behavior in the absence of free tubulin. Microtubule breakage in the absence of free tubulin is length dependent (i.e. long microtubules break faster than short microtubules) and is crucially dependent on the lattice energy. We simulated the fracture process for end-capped microtubules in the absence and presence of defects (2 defects per 16 μm shaft length, corresponding roughly to the experimentally measured incorporation frequency and microtubule length at 20 μM free tubulin). The distribution of microtubule life times to breakage was wide with typical times of the order of 10 min (Supplementary Fig. S4a). Microtubules containing defects broke faster than without defects, although the difference was small, and can be attributed rather to the presence of less stable lattice structures than to the presence of the defects themselves, i.e. the 12 protofilament lattice structure breaks faster, than the more stable 13 protofilament lattice structure. Apparently, the perturbation of the lattice structure (i.e. missing bonds at the dislocation) and the strain accumulated at the defect core was too small to initiate breakage. Typically in the simulations in the presence of defects, a single hole formed which grew rapidly in a longitudinal direction and reached a length of a few μm at breakage (Supplementary Fig. S4b). This rapid loss of dimers in a longitudinal direction reflects the lattice anisotropy in the bond energies. Dimers were lost at the defect, but the lattice was stabilized by the breathing mechanism, which led to a rapid motion of the dislocation, thereby extending the region of the 12 protofilament structure at the expense of the 13 protofilament structure. To test the model predications of breakage times we performed experiments with end stabilized microtubules (grown at 20 μM free tubulin) in the complete absence of free tubulin. We found that microtubules developed soft, flexible regions a few micrometers in length, which continued to spread along the microtubule shafts. The highly bent regions eventually broke after 10±5 min, followed by rapid shortening of the remaining microtubule ends (Supplementary Fig. S4c). The typical time scale of breakage and the size of soft regions matched well with the simulations and confirmed also the observations of Dye *et al.* [5] albeit on a shorter time scale. This indicates that

* laurent.blanchoin@cea.fr
† manuel.thery@cea.fr
‡ karin.john@univ-grenoble-alpes.fr

tubulin is lost preferentially in a longitudinal direction and in a cooperative process, as expected for an anisotropic lattice where longitudinal bonds are stronger than lateral bonds [3]. In our simulations we used a ratio of longitudinal to lateral binding energies of $\Delta G_1/\Delta G_2 = 2$. A higher ratio, as for instance used in VanBuren *et al.* [1] would lead to much longer holes at breakage, which does not agree with our experimental observations (Supplementary Fig. S4c). At this point we cannot exclude the possibility that lattice bond energies are higher than anticipated and that defects play a critical role in the fracture process. However, our model simulations naturally include the fracture process consistent with our experimental data without additional assumptions.

III. TABLES OF PARAMETER VALUES FOR MONTE-CARLO SIMULATIONS

Parameter	Explanation	Value	References/Remarks
ΔG_1	longitudinal binding energy (D-D, T-D)	-15 k_BT	similar values have been used by others [1, 6, 7] lattice anisotropy is $G_1/G_2 = G_{T1}/G_{T2} = 2$
ΔG_2	lateral binding energy (D-D, T-D)	-7.5 k_BT	
ΔG_{T1}	longitudinal stabilizing binding energy (T-T)	-3.8 k_BT	
ΔG_{T2}	lateral stabilizing binding energy (T-T)	-1.9 k_BT	
ΔG_E	entropic loss due to dimer immobilization, estimated using Eq. (1) in the main text	14.4 k_BT	estimates range from 10-20 k_BT [1, 2, 8]
ΔG_C	conformational energy penalty for a 12 protofilament lattice compared to a 13 protofilament lattice	0-0.4 k_BT	adapted for our model [9]
ΔG_S	dislocation strain energy	0-5 k_BT	adapted for our model
rate constants with $\tau \approx 0.6$ s (estimated by assuming a microtubule elongation speed of 2 μm/min at a tubulin concentration of 20 μM)			
k_{on}	on-rate constant	1 $\mu M^{-1}\,\tau^{-1}$	overall on-rate per 13 protofilament microtubule is $k_{on}^{MT} = 13\,\mu M^{-1}\,\tau^{-1}$ comparable to other studies [1, 6, 10, 11]
k_{off}	off-rate constant	1 τ^{-1}	exemplary for a GTP-dimer with one lateral and one longitudinal GTP-dimer neighbor [Eq. (1) in the main text]
k_{hy}	GTP-hydrolysis rate constant	0.6 τ^{-1}	comparable to Melki *et al.* [11]
k_{br}	breathing rate constant	1 τ^{-1}	closing rate constant k_{cl} can be obtained via Eq. (3) in the main text, varied in the range 0.1-10 τ^{-1} in Supplementary Fig. S2d

TABLE S1. Parameter values used for the Monte-Carlo simulations in Fig. 2 and Supplementary Figs. S2 and S4 unless stated otherwise (see also Methods in the main text).

Parameter	Explanation	Value	References/Remarks
ΔG_1	longitudinal binding energy (D-D, T-D)	-20 k_BT	similar values have been used by others [1, 6, 7] lattice anisotropy is $G_1/G_2 = G_{T1}/G_{T2} = 2$
ΔG_2	lateral binding energy (D-D, T-D)	-10 k_BT	
ΔG_{T1}	longitudinal stabilizing binding energy (T-T)	-3.8 k_BT	
ΔG_{T2}	lateral stabilizing binding energy (T-T)	-1.9 k_BT	
ΔG_E	entropic loss due to dimer immobilization, estimated using Eq. (1) in the main text	21.9 k_BT	estimates range from 10-20 k_BT [1, 2, 8]
ΔG_C	conformational energy penalty for a 12 protofilament lattice compared to a 13 protofilament lattice	0-0.4 k_BT	adapted for our model [9]
ΔG_S	dislocation strain energy	0-5 k_BT	adapted for our model
rate constants with $\tau \approx 0.5$ s (estimated by assuming a microtubule elongation speed of 2 μm/min at a tubulin concentration of 20 μM)			
k_{on}	on-rate constant	1 μM^{-1} τ^{-1}	overall on-rate per 13 protofilament microtubule is $k_{on}^{MT} = 13\,\mu\text{M}^{-1}\,\tau^{-1}$ comparable to other studies [1, 6, 10, 11]
k_{off}	off-rate constant	1 τ^{-1}	exemplary for a GTP-dimer with one lateral and one longitudinal GTP-dimer neighbor [Eq. (1) in the main text]
k_{hy}	GTP-hydrolysis rate constant	0.45 τ^{-1}	comparable to Melki *et al.* [11]
k_{br}	breathing rate constant	1 τ^{-1}	closing rate constant k_{cl} can be obtained via Eq. (3) in the main text

TABLE S2. Parameter values used for Monte-Carlo simulations shown in Supplementary Fig. S3 for a higher total lattice binding energy of -60 k_BT (see also Methods in the main text).

IV. DETAILED DATA OBTAINED BY CRYO-ELECTRON MICROSOCOPY

Notation of lattice conformation: N_n (N: protofilament number, n: helix start number) The 11_2 lattice is a special configuration which allows 2 different conformations, denoted as 11_2a and 11_2b (see Ref. [12]). n.d. (not determined) indicates that the lattice type could not be determined precisely.

The arrow gives precisely the direction of the transition in the direction of elongation. The directionality can be inferred from the fact that in centrosome nucleated microtubules only the plus end is growing (the minus end was attached to the centrosome). For example, a 13_3 → 12_3 transition means that the microtubule changed from the 13_3 to the 12_3 conformation during growth. A double arrow ↔ indicates that the direction of the transition with respect to the direction of elongation could not be determined.

The microtubule tip growth rates have been obtained by video microscopy data and have been given in Chrétien *et al.* [13].

A. 6.5 μM

The average growth rate of these microtubules was 0.78±0.37 μm/min, and the catastrophe frequency was 0.18 min^{-1}.

1. 6.5 μM, 3 min (mean sheet length 98 nm)

13_3: 96.667 %
Others: 3.334 %
12_2: 2605.4 nm (0.152 %)
12_3: 50055.0 nm (2.929 %)

14_3: 3857.3 nm (0.226 %)
14_4: 455.0 nm (0.027 %)

Total length: 1709.18 μm
Average protofilament number: 12.97
Percentage of modified lattices*: 0.179 % (*see Chrétien and Fuller [12])
Number of transitions: 10
Average distance between transitions: 170.9 μm
Transition types:
13_3 → 12_3: n=8
13_3 → 12_2: n=1
12_3 → 11_ (n.d.): n=1

2. 6.5 μM, 10 min

13_3: 94.667.0 %
Others: 5.333 %
12_2: 3503.5 nm (0.186 %)
12_3: 44056.0 nm (2.340 %)
14_3: 50259.0 nm (2.669 %)
14_4: 2614.0 nm (0.139 %)

Total length: 1883.11 μm
Average protofilament number: 13.00
Percentage of modified lattices: 0.325 %
Number of transitions: 4
Average distance between transitions: 470.8 μm
Transition types:
13_3 → 14_4: n=1
14_3 → 13_3: n=3

3. 6.5 μM, 20 min

13_3: 90.0 %
Others: 10.0 %
11_2b: 2204.0 nm (0.128 %)
12_3: 44177.0 nm (2.739 %)
13_2: 595.3 nm (0.035 %)
14_3: 122283.4 nm (7.099 %)

Total length: 1722.60 μm
Average protofilament number: 13.04
Percentage of modified lattices: 0.163 %
Number of transitions: 19
Average distance between transitions: 90.7 μm
Transition types:
12_3 → 13_2: n=1
12_3 → 13_3: n=1
13_3 → 12_3: n=3
13_3 → 14_3: n=5
14_3 → 13_3: n=8
14_3 → 13_2: n=1

4. 6.5 μM, 30 min

13_3: 86.667 %
Others: 11.333 %
12_3: 24062.0 nm (2.249 %)
13_2: 1194.3 nm (0.112 %)
14_2: 472.9 nm (0.044 %)
14_3: 95534.0 nm (8.929 %)

Total length: 1069.96 μm
Average protofilament number: 13.07
Percentage of modified lattices: 0.156 %
Number of transitions: 11
Average distance between transitions: 97.3 μm
Transition types:
12_3 ↔ 13_3: n=1
13_2 → 13_3: n=1
13_3 → 13_2: n=1
13_3 → 12_3: n=1
13_3 → 14_3: n=1
14_3 → 13_3: n=5
14_2 → 13_3: n=1

B. 13.0 μM

The average growth rate was 2.18±0.92 μm/min. No catastrophes.

1. 13.0 μM, 3 min (mean sheet length 209 nm)

13_3: 90.333 %
Others: 9.667 %
11_2a: 1483.6 nm (0.163 %)
11_2b: 2106.0 nm (0.231 %)
12_2: 1431.7 nm (0.157 %)
12_3: 62373.0 nm (6.842 %)
14_3: 13823.0 nm (1.516 %)
14_4: 6557.4 nm (0.719 %)
15_4: 353.9 nm (0.039 %)

Total length: 911.68 μm
Average protofilament number: 12.95
Percentage of modified lattices: 1.107 %
Number of transitions: 14
Average distance between transitions: 65.1 μm
Transition types:
11_2b → 11_2a: n=1
13_3 → 12_3: n=6
13_3 → 14_3: n=2
14_3 → 13_3: n=2
15_4 → 14_4: n=1
13_3 → 11_2b: n=1
16_(n.d.) → 15_(n.d.): n=1

2. 13.0 μM, 5 min

13_3: 89.333 %
Others: 10.667 %
12_2: 7281.5 nm (0.500 %
12_3: 79370.0 nm (5.455 %)
14_3: 60986.0 nm (4.192 %)
14_4: 6887.9 nm (0.473 %)
15_3: 504.7 nm (0.035 %)
15_4: 164.4 nm (0.011 %)

Total length: 1454.95 μm
Average protofilament number: 12.99
Percentage of modified lattices: 0.971 %
Number of transitions: 34
Average distance between transitions: 42.8 μm
Transition types:
12_2 → 13_3: n=1
12_3 → 12_2: n=1
12_3 → 13_3: n=2
12_3 → 15_3: n=1
13_3 → 12_2: n=2
13_3 → 12_3: n=10
13_3 → 14_3: n=9
14_3 → 13_3: n=5
14_4 → 13_3: n=1
14_3 → 15_3: n=1
15_4 → 14_4: n=1

3. 13.0 μM, 10 min

13_3: 84 %
Others: 16.0 %
12_2: 2128.4 nm (0.241 %)
12_3: 21817.0 nm (2.469 %)
13_2: 811.0 nm (0.092 %)
14_3: 112474.5 nm (12.729 %)
14_4: 2688.4 nm (0.304 %)
16_3: 1453.8 nm (0.165 %)

Total length: 883.58 μm
Average protofilament number: 13.11
Percentage of modified lattices: 0.802 %
Number of transitions: 15
Average distance between transitions: 58.9 μm
Transition types:
12_3 → 12_2: n=1
12_2 → 12_3: n=1
13_3 → 14_3: n=4
14_3 → 13_2: n=1
14_3 → 13_3: n=7
16_3 → 15_(n.d.): n=1

4. 13.0 μM, 20 min

13_3: 76 %
Others: 24.0 %
12_3: 45390.0 nm (5.597 %)
14_3:149234.1 nm (18.403 %)

Total length: 810.93 μm
Average protofilament number: 13.13
Percentage of modified lattices: 0 %
Number of transitions: 7
Average distance between transitions: 115.8 μm
Transition types:
13_3 → 12_3: n=1
13_3 → 14_3: n=3
14_3 → 13_3: n=3

5. 13.0 μM, 30 min

13_3: 74.333 %
Others: 25.667 %
12_3: 39299.0 nm (7.680 %)
14_3: 92042.0 nm (17.987 %)

Total length: 511.72 μm
Average protofilament number: 13.10
Percentage of modified lattices: 0 %
Number of transitions: 6
Average distance between transitions: 85.3 μm
Transition types:
12_3 ↔ 13_3: n=2
13_3 ↔ 14_3: n=2
14_3 → 13_3: n=2

C. 19.5 μM

The average growth rate was 3.51±0.90 μm/min. No catastrophes.

1. 19.5 μM, 2 min (mean sheet length 307 nm)

13_3: 84 %
Others: 16 %
12_2: 1689.3 nm (0.156 %)
12_3: 39846.0 nm (3.691 %)
13_2: 500.2 nm (0.046 %)
14_3: 108989.4 nm (10.097 %)
14_4: 18321.0 nm (1.697 %)
15_3: 1440.0 nm (0.133 %)
15_4: 855.2 nm (0.079 %)
16_4: 1068.4 nm (0.100 %)

Total length: 1079.43 μm
Average protofilament number: 13.09
Percentage of modified lattices: 1.899 %
Number of transitions: 38

Average distance between transitions: 28.4 μm
Transition types:
13_2 → 14_3: n=1
13_3 → 12_3: n=1
13_3 → 14_3: n=8
14_3 → 12_2: n=1
14_3 → 13_3: n=15
14_4 → 13_3: n=3
14_3 → 14_4: n=2
14_3 → 15_3: n=3
15_3 → 13_2: n=1
15_3 → 14_3: n=2
15_3 → 16_4: n=1

2. 19.5 μM, 3 min (mean sheet length 312 nm)

13_3: 86.667 %
Others: 13.333 %
10_2: 501.7 nm (0.051 %)
11_2b: 3209.4 nm (0.329 %)
12_2: 7744 nm (0.793 %)
12_3: 50296.0 nm (5.152 %)
13_2: 900.3 nm (0.092 %)
14_3: 61390.0 nm (6.288 %)
14_4: 4479.1 nm (0.459 %)
15_4: 1648.6 nm (0.169 %)

Total length: 976.27 μm
Average protofilament number: 13.00
Percentage of modified lattices: 1.673 %
Number of transitions: 44
Average distance between transitions: 22.2 μm
Transition types:
12_3 → 13_3: n=1
12_2 → 12_3: n=1
12_3 → 13_3: n=1
13_2 → 14_3: n=1
13_3 → 12_3: n=3
13_3 → 12_2: n=2
13_3 → 13_2: n=1
13_3 → 14_4: n=1
13_3 → 14_3: n=18
13_3 → 11_2b: n=1
14_3 → 13_3: n=11
14_3 → 14_4: n=1
14_3 → 15_4: n=1
15_4 → 13_3: n=1

V. FREE TUBULIN INCORPORATION USING TICTAC BUFFER

To test the robustness of our TIRF *in vitro* setup, we performed the incorporation experiment in an alternative buffer (Tic Tac buffer, see Supplementary Methods), yielding comparable incorporation frequencies, 0.04 μm^{-1} */3.9 and 0.09 μm^{-1} */3.3, for microtubules grown at 20 μM and 32 μM free tubulin, respectively (see Supplementary Fig. S6).

VI. FREE TUBULIN INCORPORATION INTO MICROTUBULES GROWN IN XENOPUS EGG EXTRACT

In order to further challenge our model of spontaneous lattice turnover, we tested whether turnover occurs in a physiological context using *Xenopus* egg extract cytoplasm. We used the same set-up as shown in Fig. 1a for *in vitro* experiments, except that the elongation mix was composed of approximately 20 μM endogenous *Xenopus* tubulin (supplemented with 1 μM red tubulin) along with the whole egg cytoplasm content (Supplementary Fig. S7a, step I). After washout of the extract, microtubules were capped by GMPCPP in the presence of green fluorescent tubulin, then exposed to 14 μM free green-labeled tubulin in solution, washed again and inspected for tubulin incorporation at the shaft (Supplementary Fig. S7a, steps II-IV). Microtubules grown in *Xenopus* egg extract showed incorporation of free tubulin with a typical spatial frequency of 0.09 μm^{-1} */2.8 (Supplementary Fig. S7b), comparable to microtubules grown *in vitro* (Figs. 1c and 4c). Furthermore, the typical frequency matches well with earlier measured frequencies of dislocation defects for microtubules grown in cell free *Xenopus* egg extract (~0.04 μm^{-1}, see Table II in Chretien *et al.* [14]). Note, that during elongation in the *Xenopus* egg extract microtubules are exposed to microtubule associated proteins (MAPs) and may be subjected to mechanical forces induced by molecular motors. However, any nanoscale damage left by severing enzymes has been repaired rapidly within a minute [15] and microtubules with severe damage were lost during washout. A low fraction of MAPs might still be bound to the microtubules after washout of the extract and therefore present during the tubulin incorporation phase. Nevertheless, this experiment shows, that tubulin turnover takes place, despite the presence of cellular proteins and it indicates that the lattice turnover that we characterized *in vitro* is likely to occur *in vivo* as well.

VII. QUANTIFICATION OF THE NUMBER OF INCORPORATED DIMERS AT INCORPORATION SITES

In a last set of experiments we tried to quantify the order of magnitude of the number of incorporated dimers at incorporation sites. To that end we grew end-stabilized microtubules, which contained a short stretch of green fluorescently labeled tubulin (10 %) as reference stretch and performed the incorporation experiment (Supplementary Fig. S8a). We then used the fluorescence of the reference stretch to estimate the number of fluorescent dimers in the incorporation site (see Supplementary Methods). Typically, the incorporation spots were small in the range $\leq 1\,\mu$m and contained several tens of fluorescent dimers (Supplementary Fig. S8b). Although this experiment can only give a crude estimate, it confirms, that only a small fraction of the microtubule cross section participates in the turnover, i.e. the elongation of a single protofilament is a plausible scenario.

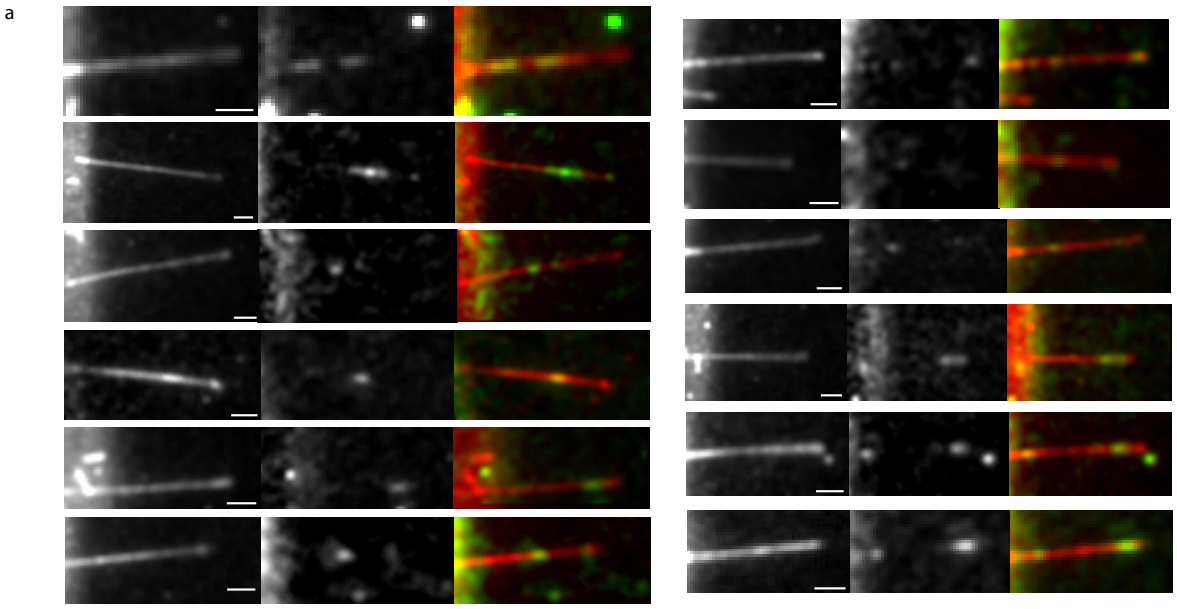

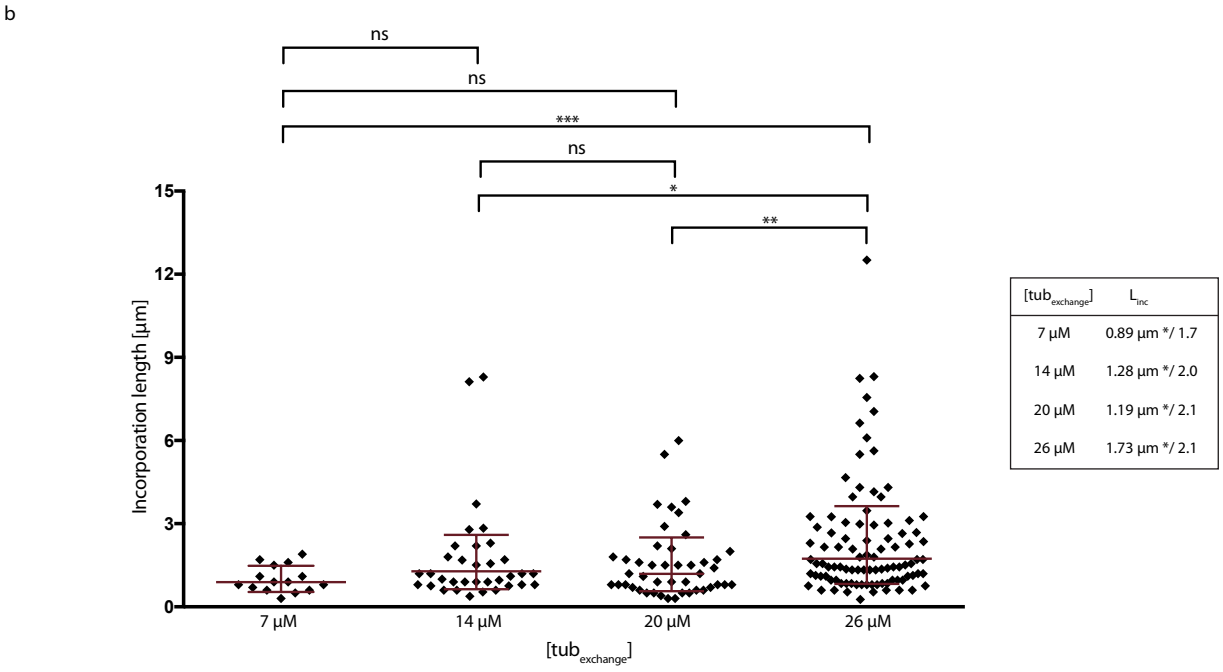

FIG. S1. (a) Examples of red microtubules showing spots of incorporated green tubulin along the lattice. The concentration of free tubulin at growth and incorporation was 20 μM. (b) Distribution of the length of incorporation spots of free tubulin into GDP-microtubules for a concentration of free tubulin at incorporation as indicated in the abscissa. The tubulin concentration at growth was 20 μM. The table summarizes the geometric mean */ sd factor of the size distribution of incorporation spots. The total number of incorporation spots and the total length of microtubules analyzed correspond to the data given in Fig. 1c. The p-values are 0.001, 0.02, and 0.008 for the pairs (7 μM, 26 μM), (14 μM, 26 μM) and (20 μM, 26 μM). All other differences are not significant.

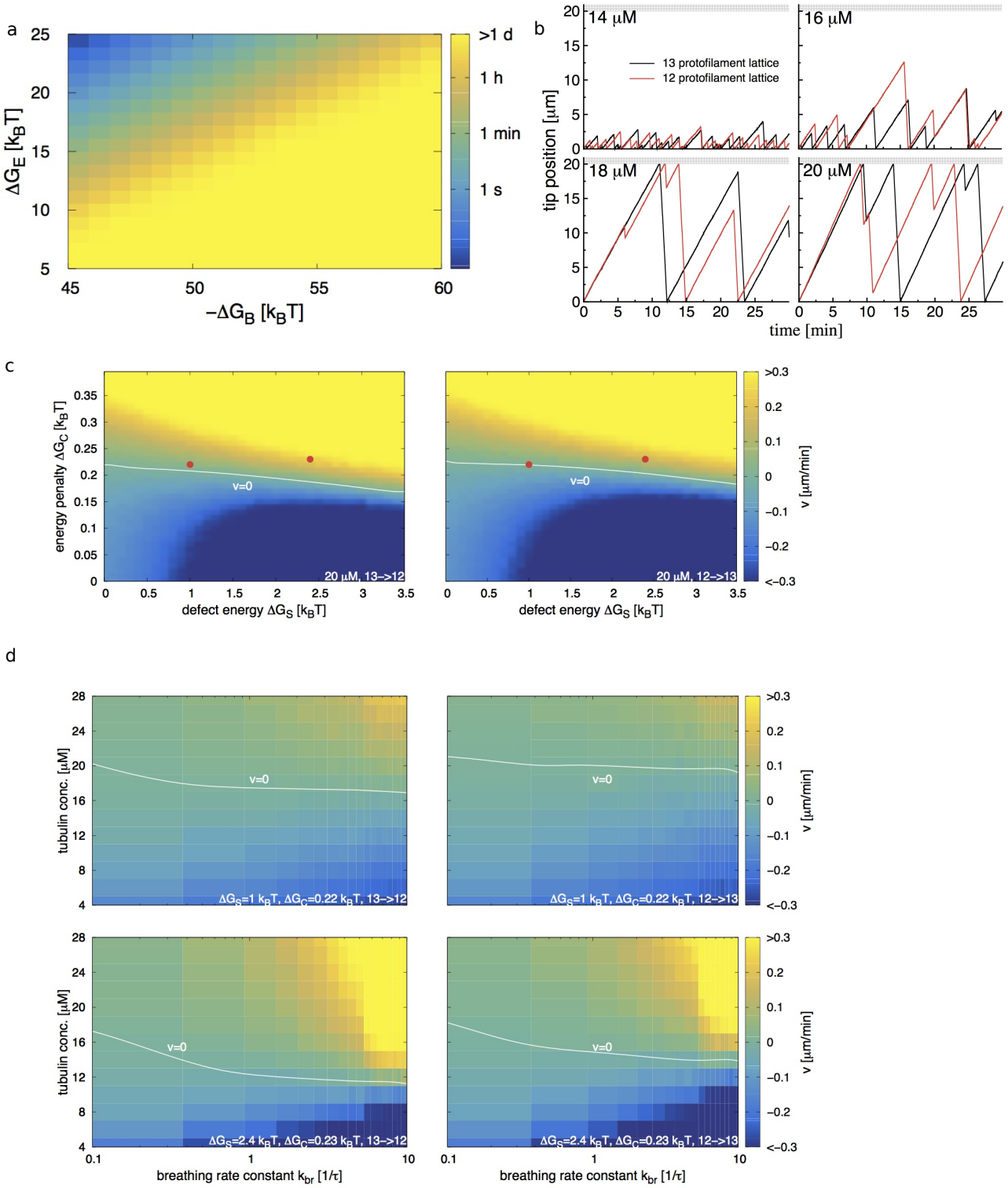

FIG. S2. (a) Phase diagram for the estimated typical time τ for a dimer to leave the intact lattice depending on the total binding energy ΔG_B and the entropic penalty for immobilizing a dimer in the lattice ΔG_E using the relation $1/\tau = k_{on} c_0 N e^{(\Delta G_B + \Delta G_E)/k_B T}$ with the on-rate constant k_{on}=5 x 10^6 M^{-1} s^{-1}, the standard concentration c_0=1 M and the number of dimers N=13*125*20=32500 in a 20 μm long microtubule. (b-d) Monte Carlo simulations of the microtubule tip and the shaft. (caption continues on next page)

FIG. S2. (b) (+)-end dynamics of the 13 (black line) and the 12 protofilament lattice (red line) at the free tubulin concentrations indicated in the legends. The growth is limited to a length of 20 μm indicated by the grey horizontal bar in each plot, beyond which no dimer addition takes place. Note, that in our experimental conditions, at 14 μM free tubulin, microtubules are short and catastrophes are frequent. (c) Phase diagrams of defect dynamics depending on the conformational energy penalty ΔG_C and the defect strain energy ΔG_S for a free tubulin concentration of 20 μM. Shown are the phase diagrams of a 13→12 (left) and a 12→13 (right) transition. (d) Phase diagrams of defect dynamics at 13→12 (left plots) and 12→13 (right plots) transitions depending on the breathing rate constant k_{br} (τ=0.6 s) and the free tubulin concentration. The defect strain energy ΔG_S and the conformational energy penalty ΔG_C is indicated in the bottom of each phase diagram. The color code in (c,d) indicates the speed of motion of the dislocation along the microtubule axis in μm/min. Note, that a positive speed $v > 0$ indicates a net elongation of the free profofilament end at the dislocation, which gets visible as incorporation spots in experiments. The white line indicates a stationary dislocation with $v = 0$. The red dots in (c) indicate the parameter combinations for the simulated kymographs of Fig. 2 e and f. Remaining parameters are as in Supplementary Table S1 and ΔG_C=0 in (b).

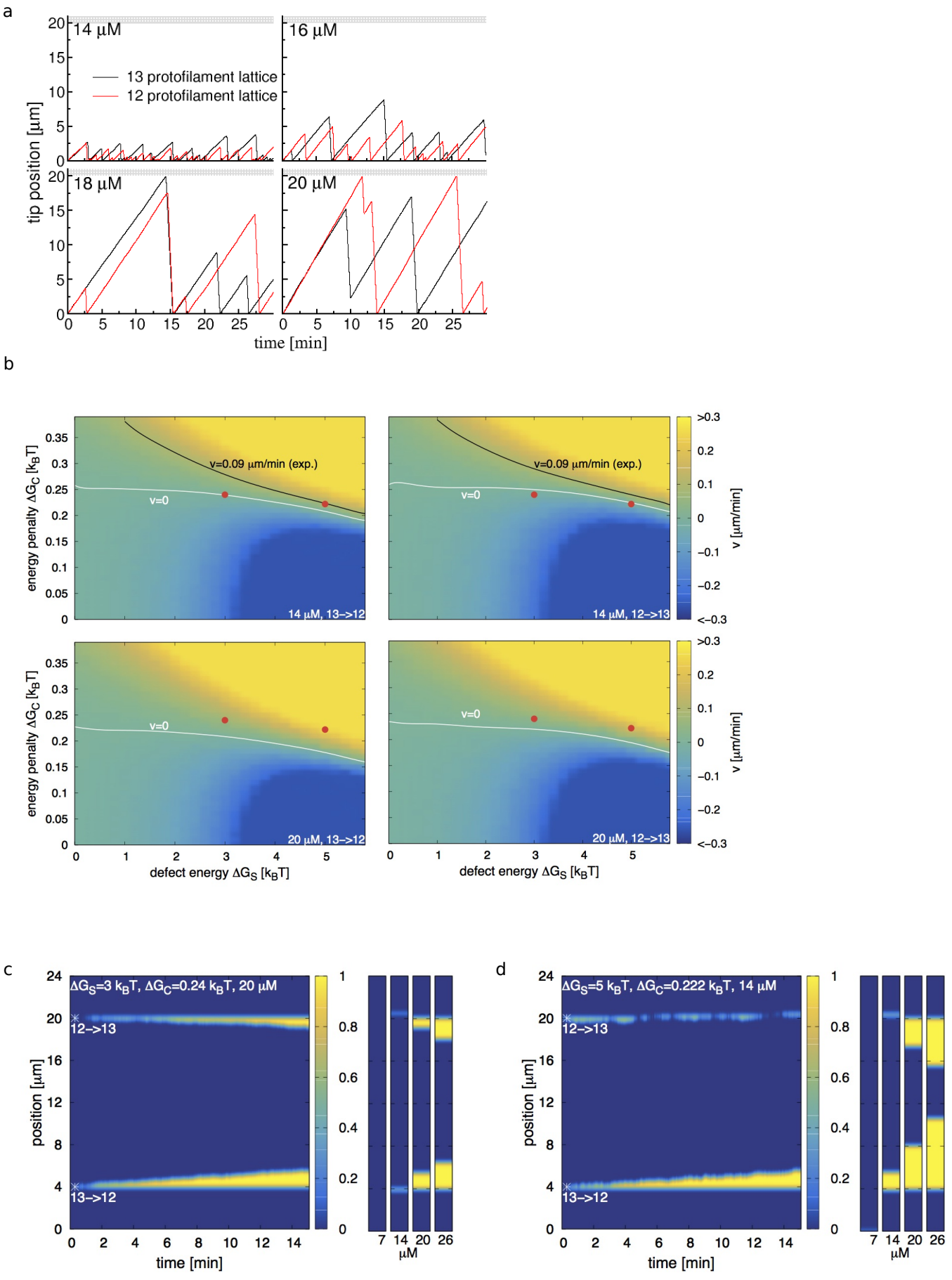

FIG. S3. (caption see next page)

FIG. S3. Monte Carlo simulations of the microtubule tip and lattice dynamics using an alternative parameter set with a high total binding energy $\Delta G_B = -60\,k_BT$. (a) Tip dynamics of the 13 (black lines) and the 12 protofilament lattice (red lines) at the free tubulin concentrations indicated in the legends. The growth is limited to a length of $20\,\mu$m indicated by the grey horizontal bar in each plot, beyond which no dimer addition takes place and catastrophe is thus induced. (b) Phase diagrams of defect dynamics at 13→12 (left) and 12→13 (right) transitions depending on the defect strain energy ΔG_S and the conformational energy penalty ΔG_C for two different free tubulin concentrations ($14\,\mu$M and $20\,\mu$M) as indicated at the bottom of each phase diagram. The color code indicates the velocity of motion of the defect. For $v > 0$ free tubulin is incorporated, whereas for $v < 0$ the additional protofilament of the 13 protofilament lattice is depolymerizing. The black line with $v = 0.09\,\mu$m/min corresponds to the experimentally measured dislocation speed at $14\,\mu$M free tubulin. The red dots indicate the parameter combinations used in the simulations in (c,d). (c,d) Simulated kymographs of free tubulin incorporation into the lattice using parameter values indicated by the red dots in (b) and as indicated at the top of each kymograph. The original positions of the lattice defects are indicated by asterisks. Shown are a 13→12 (bottom) and 12→13 (top) transition. The small graphs to the right of each kymograph show the appearance of the microtubules after 15 min at the free tubulin concentration indicated below each graph. Remaining parameters are as in Supplementary Table S2 and $\Delta G_C = 0$ in (a).

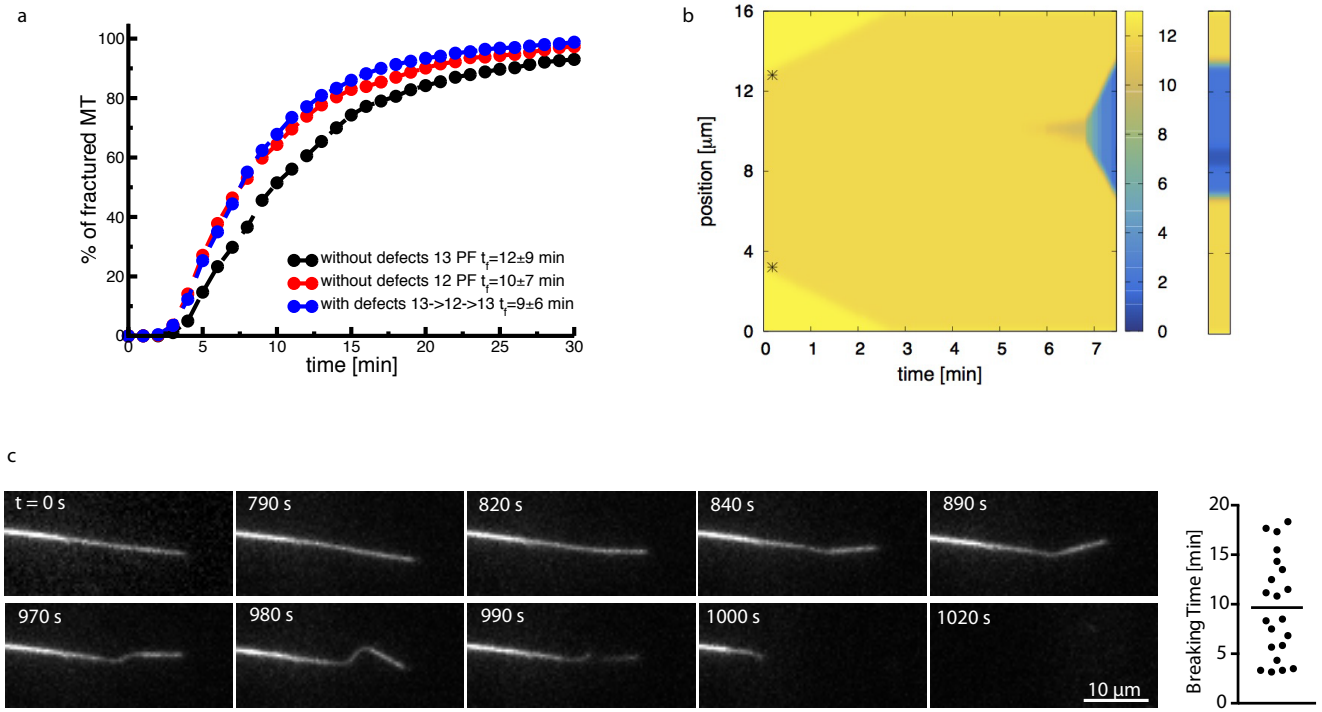

FIG. S4. Monte Carlo simulations (a,b) and experiments (c) of microtubule breakage in the absence of free tubulin. (a) Cumulative distribution of microtubule fracture times for 16 μm long end-stabilized microtubules without defects in the 13 and 12 protofilament lattice conformation and for microtubules containing 2 defects and the two different lattice conformations (each lattice conformation is 8 μm long). The legends indicate the mean time to fracture. (b) Typical example of fracture of a 16 μm long end-stabilized microtubule containing 2 defects, whose initial position is marked by the black asterisks. The color code indicates the number of occupied lattice sites per helical turn. The motion of the defect is visible by a slight change in the yellow color between 13 and 12 dimers per helical turn. The graph on the right shows the final state of the microtubule at fracture. Parameters for (a,b) are as in Supplementary Table S1 and $\Delta G_S = 2.4\, k_B T$, $\Delta G_C = 0.23\, k_B T$. (c) Sequence of experimental images showing a capped microtubule in the absence of free tubulin, which develops a soft region that extends several μm along the microtubule before breakage. The graph on the right shows the time that microtubules survive before breaking, the bar represents the mean survival time.

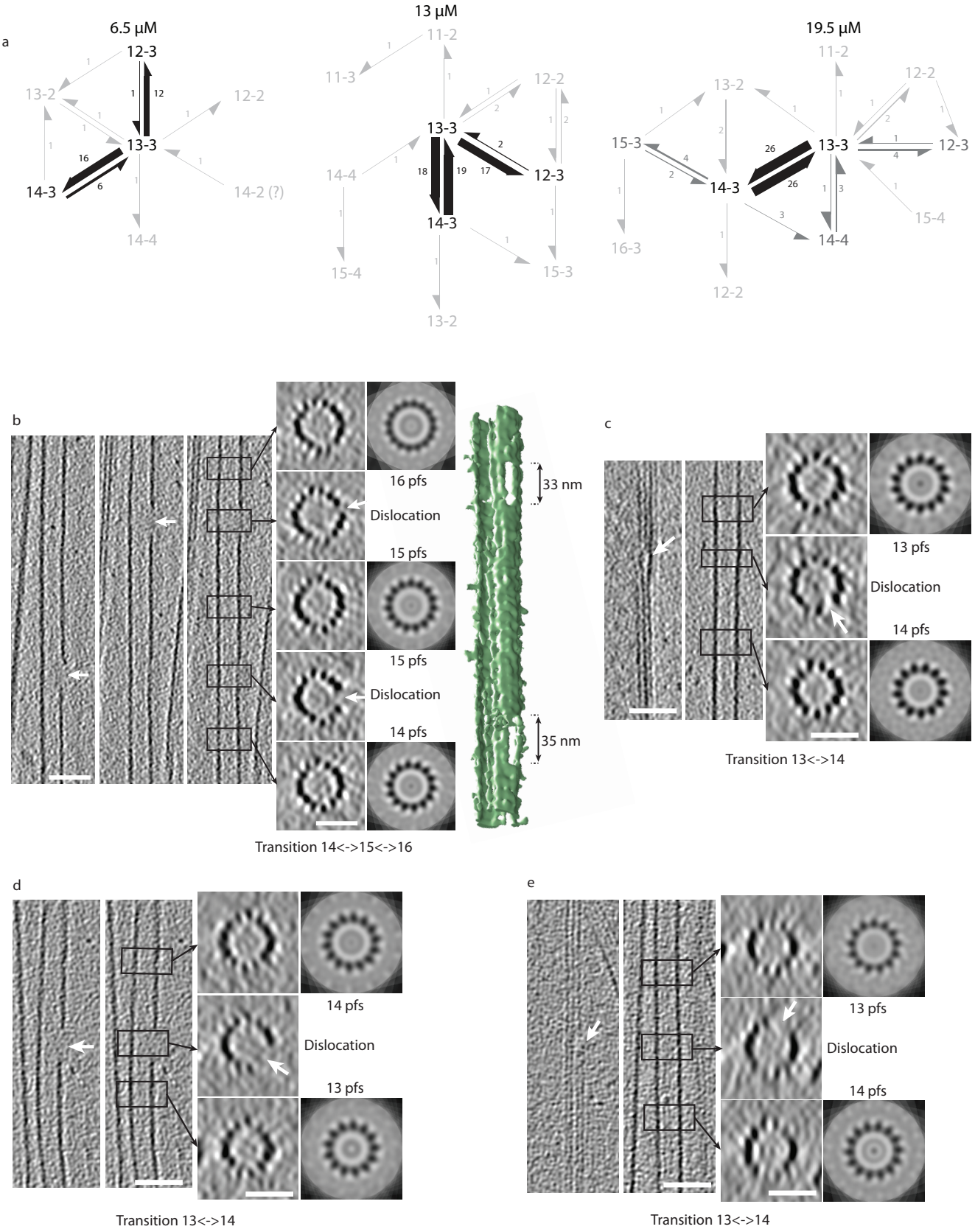

FIG. S5. (caption see next page)

FIG. S5. Dislocation defects in the microtubule lattice detected by cryo-electron microscopy. (a) Schema of the lattice transitions observed by cryo-electron microscopy. N_n denotes a N protofilament lattice with a n-helix start number. The numbers on the arrows indicate the numbers of observed transitions. The arrows indicate the transitions occurring in the direction of growth. The most prominent lattice conformations and transitions are shown in black (the rest in gray). The thickness of the arrows correlates with the frequency of transitions. (b-e) Cryo-electron tomograms of protofilament number transitions. The left panels show longitudinal slices through the microtubule in the transition region whereas the right panels show transverse sections. The transverse sections are averaged over the height of the black rectangles shown in the longitudinal sections (corresponding regions are indicated by black arrows) and correspond to *N*-fold rotational averages of the closed microtubule regions (*N* denotes the protofilament number). White arrows indicate the free end of a protofilament (dislocation) with the accompanying gap in the lattice at the transition. The scale bars are 50 nm for longitudinal and 25 nm for transverse sections. (b) A 15↔16 and 14↔15 protofilament number transitions in close proximity in the same microtubule. The left most and central longitudinal sections were imaged at different depths to show the gaps in the transition regions. The central and right most longitudinal sections are identical. The image to the far right shows the 3D rendering (visualized under UCSF Chimera [16]) of the microtubule with the dislocations at the edge the microtubule. Two gaps in the lattice with approximate lengths of 33 nm and 35 nm are clearly visible. (c-e) Three examples of 14↔13 protofilament number transitions. The left longitudinal section shows a cut through the transition region, whereas the right longitudinal section shows a cut through a central part of the microtubule. In (d) both longitudinal sections are identical.

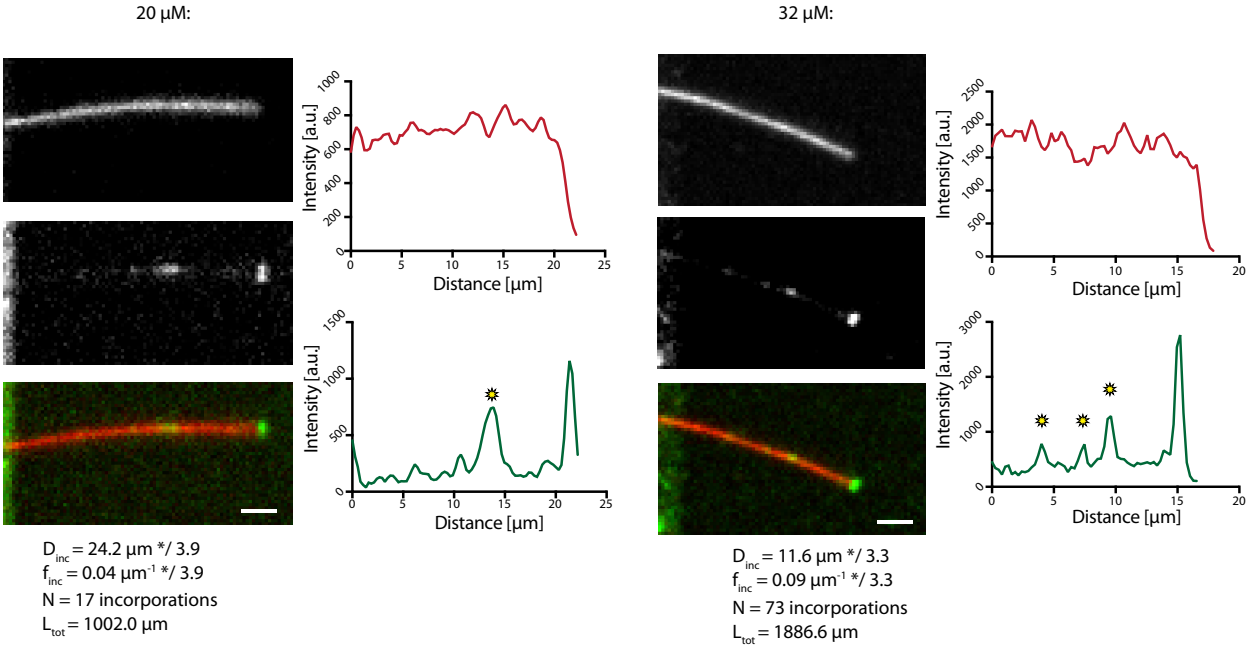

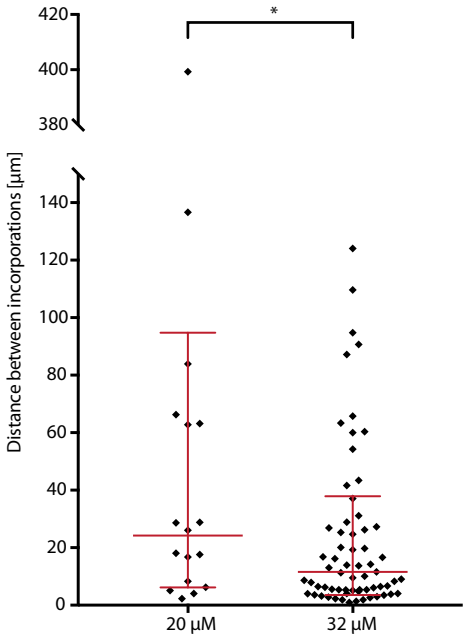

FIG. S6. Incorporation of free tubulin into GDP-microtubules using a different buffer (Tic Tac buffer instead of BRB buffer). Microtubules were grown in Tic Tac buffer at 20 μM (left) and 32 μM (right) free tubulin concentration before they were capped with GMPCPP and exposed to 14 μM of green-fluorescent free tubulin. The images and line scans represent typical examples of tubulin incorporation into the shaft. The average distance (D_{inc}) and frequency (f_{inc}) between incorporation spots is indicated below the images as geometric mean */sd factor. N and L_{tot} denote the total number of incorporation spots and the total length of microtubules analyzed, respectively. Scale bars: 3 μm. The graph shows the distribution of distances between incorporation spots after concatenating all microtubules in a random order. The red bars indicate the geometric mean /*sd factor. The p-value is 0.047.

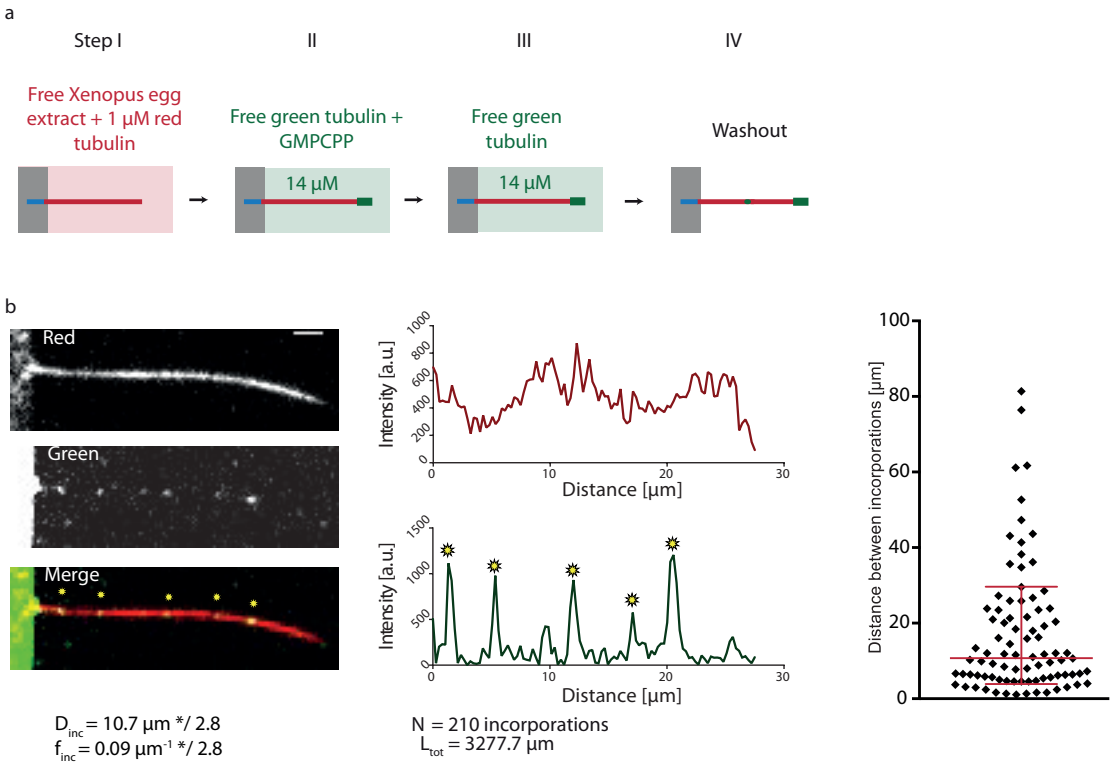

FIG. S7. Incorporation of free tubulin into microtubules grown in *Xenopus* egg extract. (a) Schematic representation of the experimental setup to test the role of the microtubule growth medium on tubulin turnover in the microtubule lattice. Microtubules were grown in cell free *Xenopus* egg extract supplemented by 1 μM red-fluorescent free tubulin (step I) before washing and capping with GMPCPP (14 μM green tubulin, step II). Microtubules were then exposed to 14 μM green-fluorescent free tubulin for 15 min (step III) before a final washout and subsequent observation (step IV). (b) The images and line scans show an example of a microtubule grown in cell free *Xenopus* egg extract. The average distance D_{inc} and frequency f_{inc} (geometric mean */sd factor) between sites of tubulin incorporation are shown below. N and L_{tot} denote the total number of incorporations and the total length of microtubules analyzed, respectively. Scale bar: 3 μm. The graph shows the distribution of distances between incorporation sites after concatenating all microtubules in a random order. The red bars represents the geometric mean */sd factor.

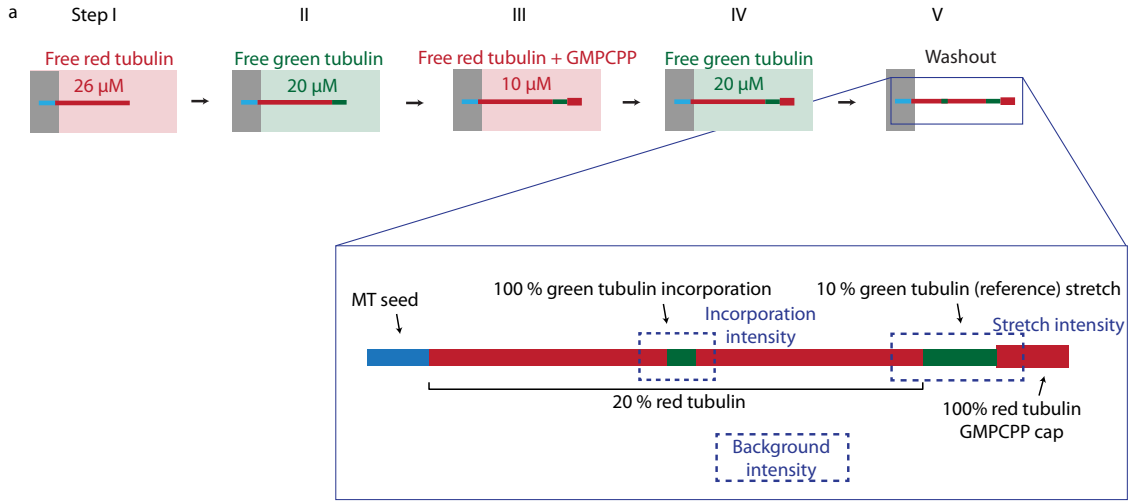

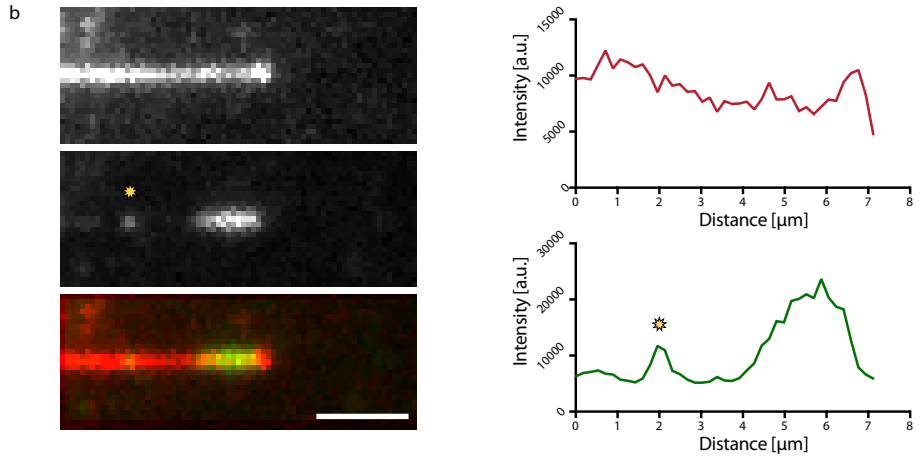

Number of incorporated dimers

Microtubule \ Laser intensity	High	Low
1	42 ± 9	44 ± 9
2	62 ± 11	76 ± 14
3	6 ± 3	9 ± 5
4	23 ± 12	32 ± 16
5	21 ± 9	21 ± 13
Mean	31 ± 22	36 ± 26

FIG. S8. Quantification of the approximate number of tubulin dimers at incorporation sites. (a) Schematic representation of the experimental setup used to quantify the number of fluorescent tubulin dimers at incorporation sites. Microtubules were grown with red-fluorescent tubulin at a concentration of 26 μM (step I) then further elongated with 20 μM green tubulin (10 %, "reference stretch", step II), before they were capped with GMPCPP (step III) and exposed to 20 μM of green-fluorescent free tubulin (step IV). After 15 min, the free green tubulin was washed out (step V) to reveal spots of green tubulin along the red microtubule, which were compared to the "reference stretch" to estimate the number of fluorescent dimers (see Methods). (b) Example images and line scans of green and red fluorescence along a microtubule grown with the protocol shown in (a). The table summarizes the estimates of incorporated dimers for two different laser intensities (low, high). Values are mean ± sd calculated from 10 individual images, respectively. The length of the incorporation spots was $\leq 1\,\mu$m. Scale bar: 3 μm.

VIII. SUPPLEMENTARY METHODS

A. Microtubule growth on micropatterns using Tic Tac buffer

The PDMS chip was placed on a micropatterned cover glass and fixed on the microscope stage. The chip was perfused with neutravidin (25 μg/ml in BRB80; Pierce), then washed with HKEM (10 mM Hepes pH7.2; 5 mM $MgCl_2$; 1 mM EGTA ; 50 mM KCl), passivated for 20 s with PLL-g-PEG (Pll 20K-G35-PEG2K, Jenkam Technology) at 0.1 mg/ml in 10 mM Na-Hepes (pH = 7.4), and washed again with HKEM. Microtubule seeds were flowed into the chamber at high flow rates perpendicularly to the micropatterned lines to ensure proper orientation of the seeds. Non-attached seeds were washed out immediately using HKEM supplemented with 1 % BSA. Seeds were elongated with 20 μM tubulin (20 % labeled) in Tic Tac (16 mM Pipes pH 6.9; 10 mM Hepes; 5 mM $MgCl_2$; 1 mM EGTA; 50 mM KCl) supplemented with an oxygen scavenger cocktail (20 mM DTT, 1.2 mg/ml glucose, 8 μg/ml catalase and 40 μg/ml glucose oxidase), 0.1 % BSA, 0.025 % methyl cellulose (1500 cp, Sigma) and 1 mM GTP at 37 °C. GMPCPP caps were grown by supplementing a mix containing 14 μM of tubulin (100 % labeled) in HKEM supplemented with an oxygen scavenger cocktail (20 mM DTT, 1.2 mg/ml glucose, 8 μg/ml catalase and 40 μg/ml glucose oxidase), 0.1 % BSA, 0.025 % methyl cellulose (1500 cp, Sigma) and 0.5 mM GMPCPP (Jena Bioscience) at 37 °C. For incorporation experiments, the same buffer as for elongation was used, supplemented by 14 μM tubulin (100 % labeled, green fluorescent, labeling ratio of about 2 fluorophores per dimer). Microtubules were incubated in this buffer for 15 min at 37 °C before replacing it with washing buffer for imaging.

B. Microtubule growth on micropatterns using cell free *Xenopus* egg extract

The PDMS chip was placed on a micropatterned cover glass and fixed on the microscope stage. The chip was perfused with neutravidin (25 μg/ml in BRB80; Pierce), then washed with HKEM (10 mM Hepes pH 7.2; 5 mM $MgCl_2$; 1 mM EGTA; 50 mM KCl), passivated for 20 s with PLL-g-PEG (Pll 20K-G35-PEG2K, Jenkam Technology) at 0.1 mg/ml in 10 mM Na-Hepes (pH 7.4), and washed again with HKEM. Microtubule seeds were flowed into the chamber at high flow rates perpendicularly to the micropatterned lines to ensure proper orientation of the seeds. Non-attached seeds were washed out immediately using HKEM supplemented with 1 % BSA. Seeds were elongated with *Xenopus* egg extract supplemented with 1 μM of tubulin (100 % labeled, red fluorescent) in BRB80 at 37 °C. *Xenopus* egg extract was prepared as described by Murray *et al.* [17]. CSF arrested extracts were induced to interphase by addition of 0.5 mM $CaCl_2$ for 45 minutes. In that type of "low speed" extracts, microtubule concentration is estimated to range around 20 μM [18]. Dynein-dependent motility was then inhibited with 0.5 mM vanadate, and microtubule nucleation was facilitated by addition of 11 μM RanQ69L as described by Petry *et al.* [19]. GMPCPP caps were grown by supplementing a mix containing 14 μM of tubulin (100 % labeled, green fluorescent) in HKEM supplemented with an oxygen scavenger cocktail (20 mM DTT, 1.2 mg/ml glucose, 8 μg/ml catalase and 40 μg/ml glucose oxidase), 0.1 % BSA, 0.025 % methyl cellulose (1500 cp, Sigma) and 0.5 mM GMPCPP (Jena Bioscience) at 37 °C. For incorporation experiments, the same buffer as for capping was used, supplemented by 14 μM tubulin (100 % labelled, green fluorescent, labeling ratio of about 2 fluorophores per dimer) and we replaced 0.5 mM GMPCPP by 1 mM GTP. Microtubules were incubated in this buffer for 15 min at 37 °C before replacing it with washing buffer for imaging.

C. Estimation of the number of fluorescent dimers at incorporation sites

From the length (FWHM), the length of a tubulin dimer (L), and the integral (I_{total}) of the fluorescence intensity of a 10 % fluorescently labeled microtubule stretch we can estimate the fluorescence intensity emitted by a singe dimer (I_{dimer}) as $I_{dimer}=I_{total}*L/(FWHM*13*0.1)$, assuming a 13 protofilament structure. From the integral of the fluorescence (I_{inc}) at the incorporation spot we can deduce the number of incorporated dimers as $N_{inc}=I_{inc}/I_{dimer}$. Measurements were performed at two different laser intensities to get a rough error estimate.

[1] V. VanBuren, D. J. Odde, and L. Cassimeris, Proc. Natl. Acad. Sci. USA **99**, 6035 (2002), doi:10.1073/pnas.092504999.
[2] J. Howard, Mechanics of motor proteins and the cytoskeleton (Sinauer associates Sunderland, MA, 2001).
[3] D. Sept, N. A. Baker, and J. A. McCammon, Prot. Sci. **12**, 2257 (2003), doi:10.1110/ps.03187503.
[4] T. Mitchison and M. W. Kirschner, Nature **312**, 237 (1984), doi:10.1038/312237a0.
[5] R. B. Dye, P. F. Flicker, D. Y. Lien, and R. C. Williams, Cell Mot. Cytoskel. **21**, 171 (1992), doi:10.1002/cm.970210302.
[6] M. K. Gardner, B. D. Charlebois, I. M. Jánosi, J. Howard, A. J. Hunt, and D. J. Odde, Cell **146**, 582 (2011), doi:10.1016/j.cell.2011.06.053.

[7] Z. Wu, H.-W. Wang, W. Mu, Z. Ouyang, E. Nogales, and J. Xing, PLoS ONE **4**, e7291 (2009), doi:10.1371/journal.pone.0007291.
[8] H. P. Erickson, J. Mol. Biol. **206**, 465 (1989).
[9] V. Hunyadi, D. Chrétien, and I. M. Jánosi, J. Mol. Biol. **348**, 927 (2005), doi:10.1016/j.jmb.2005.03.019.
[10] R. A. Walker, E. T. O'Brien, N. K. Pryer, M. F. Soboeiro, W. A. Voter, H. P. Erickson, and E. D. Salmon, J. Cell Biol. **107**, 1437 (1988), doi:10.1083/jcb.107.4.1437.
[11] R. Melki, S. Fievez, and M.-F. Carlier, Biochem. **35**, 12038 (1996).
[12] D. Chrétien and S. D. Fuller, J. Mol. Biol. **298**, 663 (2000), doi:10.1006/jmbi.2000.3696.
[13] D. Chrétien, S. D. Fuller, and E. Karsenti, J. Cell Biol. **129**, 1311 (1995), doi:10.1083/jcb.129.5.1311.
[14] D. Chrétien, F. Metoz, F. Verde, E. Karsenti, and R. H. Wade, J. Cell Biol. **117**, 1031 (1992), doi:10.1083/jcb.117.5.1031.
[15] A. Vemu, E. Szczesna, E. A. Zehr, J. O. Spector, N. Grigorieff, A. M. Deaconescu, and A. Roll-Mecak, Science **361**, eaau1504 (2018), doi:10.1126/science.aau1504.
[16] E. F. Pettersen, T. D. Goddard, C. C. Huang, G. S. Couch, D. M. Greenblatt, E. C. Meng, and T. E. Ferrin, J. Comput. Chem. **25**, 1605 (2004), doi: 10.1002/jcc.20084.
[17] A. Murray, Meth. Cell Biol. **36**, 581 (1991).
[18] S. F. Parsons and E. D. Salmon, Cell Mot. Cytoskel. **36**, 1 (1997), doi:10.1002/(SICI)1097-0169(1997)36:1¡1::AID-CM1¿3.0.CO;2-E.
[19] S. Petry, A. C. Groen, K. Ishihara, T. J. Mitchison, and R. D. Vale, Cell **152**, 768 (2013), doi:10.1016/j.cell.2012.12.044.